Analysis of Spectral Transmission in Si Solar Cell With Pyramidal Texturization by Using PC3S Simulation

Ahmad Rujhan Mohd Rais
Universiti Kebangsaan Malaysia Institut Penyelidikan Tenaga Suria
Nurul Aqidah Mohd Sinin
Universiti Kebangsaan Malaysia Institut Penyelidikan Tenaga Suria
Suhaila Sepeai (suhailas@ukm.edu.my)
Universiti Kebangsaan Malaysia Institut Penyelidikan Tenaga Suria
Mohd Adib Ibrahim
Universiti Kebangsaan Malaysia Institut Penyelidikan Tenaga Suria
Saleem H. Zaidi
Universiti Kebangsaan Malaysia Institut Penyelidikan Tenaga Suria
Kamaruzzaman Sopian
Universiti Kebangsaan Malaysia Institut Penyelidikan Tenaga Suria

Research Article

Keywords: Crystalline, Pyramidal Texturing, Scattering, Two-Dimensional Texturing

Posted Date: July 30th, 2021

DOI: https://doi.org/10.21203/rs.3.rs-741857/v1

Abstract

Management of light is a crucial task in solar cell design and structure because it increases the path length of the light inside, which in turn increases the probability of electron-hole pair generation. This study addresses the impact of a pyramidal textured structure on spectral transmission in the morphology of silicon. The morphology of silicon wafers was investigated using PC3S spectral transmission software to study the spectral transmission, reflectance, collection probability, mobility, carriers, electric field, velocity, current and surface recombination. Spectral transmission on the front surface with pyramidal texture showed a better transmission percentage than the planar surface. The texture with a depth of 20 μm and base length of 20 μm exhibited good performance in front spectral transmission, spectral reflectance, electric field, velocity, current and surface recombination from the top to the bottom of the sample. The planar surface had more reflectance and lower collection probability than the other pyramidal textured samples due to its low mobility, carriers, electric field, velocity and current but high surface recombination.

Introduction

Texturization is the formation of a rough surface on silicon wafer, and it can be performed through the texturing process. This process increases the surface area of silicon solar cells that can extract and trap more photon energy than a planar surface can. Increasing the surface area of silicon solar cells enhances the performance of the solar cells and can produce an improved photoelectric output. Light trapping can be increased by creating a textured surface on a silicon solar cell via suitable texturing procedures [1]. By contrast, a planar surface silicon solar cell has high optical losses, which affect the entire performance of the solar cell considerably [2]. The high reflective index of crystalline silicon causes huge optical losses of around 30%–40%, which are the main factors that degrade solar cell performance [3]. Incident photons are reflected in planar surface silicon solar cells rather than being fully absorbed internally by the solar cells. By contrast, a textured surface significantly reduces optical losses by trapping incident photons inside the textured structures, thus improving the performance of the solar cell. In addition, it overcomes all of the main problems related to production costs [3–4].

Texturization in the form of a homogenous and uniform pyramidal distribution can improve the minority carriers' lifetime and overcome optical losses, thereby reducing recombination losses [5]. Texturization with a pyramidal structure by using alkaline solutions can decrease the overall reflection losses to below 15%. Anti-reflective coatings (ARCs) include silicon oxide (SiO_2) and silicon nitride (SiN_x) for front surfaces. These films produce a good outcome in improving optical transmittance (~90%) in the wavelength range of 400–1100 nm. Adding texturization and anti-reflective coatings reduces reflectance losses and increases the overall performance of silicon solar cells.

Extensive research has been conducted on texturization to improve optical losses caused by surface reflectance [6–9]. The majority of recent studies discussed the effect of texturization on minority carrier lifetime in monocrystalline silicon solar cells. E. Yu Plotnikova et al. [10] conducted simulation studies on

textured solar cells by using TCAD modelling with different textured structures and concluded that solar cells with small and large pyramidal textures perform better than flat structures. Although this study evaluated electrical performance, optical performance on textured surfaces was not thoroughly discussed. Chen Jin et al. [11] studied the impact of substrate thickness and front surface recombination velocity on the overall photo-electrical performance of an interdigitated back contact (IBC) silicon solar cell with a random pyramidal texture by using Silvaco ATLAS simulation software. Their results proved that thinning the substrate causes losses in short-circuit current density whilst maintaining the open-circuit voltage. In addition, wafer ray tracer simulation was used to study the optical properties of the random pyramidal texture for thin substrates. Shijun Ma et al. [12] performed a theoretical study on the optical properties of black silicon nanostructures in the range of visible light to near-infrared light by using statistical programming and the numerical finite-difference time-domain (FDTD) method. These studies showed that almost 80% of incident light is redirected and subjected to internal reflection.

Furthermore, D. Pera et al. [13] implemented a numerical 3D image reconstruction algorithm with FDTD simulations to analyse the optical performance of a random pyramidal texture. FDTD was used to investigate reflectance, absorption and charge generation, and it produced accurate optical generation rates related to complex micro- and nano-textured surfaces. This method's results showed good agreement with the experimental results on effective reflectivity, spectral reflectance and spectral absorbance for the textured silicon cell. D. Shah et al. [14] conducted a simulation and experimental study on the impact of the length and reflectance of silicon nanowires (SiNWs) by using PC1D to evaluate optical performance. The optical evaluation for SiNWs was not stimulated by using PC1D, but the electrical performance of the solar cell in the simulation is close to the experimental value. Halo Dalshad Omar et al. [15] simulated light trapping on an inverted pyramidal texture by using wafer ray tracer to study the light scattering effect and electrical performance. This work used planar texture as the baseline to examine the improvement in inverted pyramids; the texture resulted in an enhancement of light absorption for all inverted pyramids compared with the planar surface.

This work focuses on the comprehensive evaluation of the optical performance of pyramidal texturization profile structures of silicon solar cell devices by using PC3S [16]. PC3S [16] simulation was performed to give insights into the physical cell structure that provides a superior, fully 3D treatment of pyramidal texturization. The simulation was built in Microsoft Excel, and all calculations were performed in a code file, which was extracted in Microsoft Excel. PC3S offers a good means of studying the physics within a texturization structure. This software was created by Paul Basore and released in December 2020.

PC3S has several solution modes that can be used to study the physics within a textured surface region. In this study, a simulation was performed by applying the bipolar mode to the voltage between the front and rear of the silicon cell, which is known as a doped emitter. The rear of the silicon cell was applied with voltage (quasi-Fermi splitting) through the floating mode. The total recombination applied in the simulation solution region was equal to the total photo-generation in the solution region; the former was applied using the open mode, which allows quasi-Fermi levels to float non-uniformly. Moreover, flat-band

mode was applied to the solution to assess the recombination losses as a function of applied voltage for the high-efficiency limit. The quasi-Fermi separation was uniform throughout. The left-to-right voltage across the solution region induced a lateral current flow, which could be used to determine the effectiveness of the sheet resistance of the textured surface known as lateral mode.

This study explored the use of the bipolar, floating, open, flat-band and lateral mode device simulators in PC3S to simulate and study the spectral transmission in 2D surface morphologies of silicon wafer. The aim is to study the mobility, carriers, surface recombination, electric field, velocity and current under various pyramidal structure sizes. The performance of the proposed device is analysed with respect to the influence of the front passivation of SiO_2 and SiN_x.

Methodology

PC3S software has five important components, namely, dashboard, device, optics, data and image. Each of these components plays an important part in studying the spectral transmission inside solar cell devices. The first part of the software, the PC3S dashboard, consists of the initial file data that can be uploaded from external sources and will be estimated by the PC3S software. This part also consists of output results from the solved external input data, which are spectral transmission, recombination, sheet Rho and graphical output of solar cell samples.

The second part, the PC3S device, presents the details of the device uploaded from the external command data into the software, which include solution volume of the device, textured patterns, diffusion doping, bulk doping, surface charge and recombination. The third part, PC3S optics, provides information on the parameter used in PC3S simulation to estimate the spectral transmission of the solar cell samples; the information consists of spectrum, surface coating, power density, absorption coefficient and index of reflection with respect to wavelength in air. The fourth part, PC3S data, calculates and produces the output data from the external command file uploaded on the PC3S dashboard. This part shows the output recombination, sheet Rho and spectral reflected, absorbed and collected. The last part, PC3S image, shows the graphical output variable as plotted on the PC3S dashboard for each calculated input datum across multiple symmetry planes of the devices.

Table 1 shows the parameter of silicon used in the simulation. Fourteen samples were investigated in this study. The details of the samples are shown in Table 2. All samples are p-type silicon wafers with width, length and height of 1.00 μm. The silicon surface was diffused with an n^+ emitter and passivated with thin interfacial oxide and positive-charge silicon nitride for SiN_x anti-reflection coating. The p-type silicon sample was used with a variable textured surface and diffused via n+ diffusion. The front surface was passivated with thin interfacial oxide and coated with anti-reflection coating of positive-charge silicon nitride. The planar surface morphology of the silicon wafer was used as the baseline to determine any improvement in the variable textured surface of the silicon cell. The period (P) of the pyramidal texture was the length from the peak of the pyramidal texture to the next peak of the pyramidal texture. Depth (D)

was the textured depth from the peak to the base of the pyramidal texture. The P and D of the pyramidal texture are shown in Fig. 1.

Figures 2(a) and 2(b) show a schematic of the device in planar and textured surface used in this study respectively. The surface morphology of the p-type wafer had two ARC layers, namely, SiO_2 and SiN, as passivation. The devices were simulated on reflected and collected light. The measurement was simulated by varying the wavelength, base length, depth and base angle of the pyramidal texture. The mobility and carriers were investigated because of their critical influence on determining the efficiency of the solar cell. Moreover, drift velocity with the presence of an electric field was investigated because of its impact on the mobility of the charge carrier.

Simulation Results And Discussion

Figures 3, 4, and 5 show the spectral transmission on the front surface morphology of the silicon wafer for textured surface with period of 4 *um,* 8 *um*, and 20 *um* respectively. The spectral transmission of B, C and D with a similar length and depth of 4, 6 and 8 um, respectively, exhibited lower spectral performance on the front surface than the planar baseline. However, the other samples showed an improvement in spectral transmission compared with the planar baseline. Sample A with a depth of 4 um exhibited better performance than Samples C (depth of 8 um) and D (depth of 10 um) with a difference of almost 40% from the visible to infrared range; the difference for B sample was around 30%. Sample A showed spectral transmission that was 15% better than that of the planar baseline in the range of 300–600 nm, whereas Samples C and D had less than 15%. Samples B, C and D had a base angle of more than 65º, which was below that of the planar baseline. The spectral transmission on the front surface was higher than that under the practical and proposed base angles of texture around 50°–55°. The base angle of the texture should be close to 50°–52° and the most commonly accepted angle of 54.74° [15, 17–19].

As shown in Figures 4 and 5, Samples E (depth of 2 um), M (depth of 20 um) and N (depth of 20 um) with a base angle below 30° manifested a low spectral transmission percentage in the solar cell devices because more reflection occurred on the front surface. The samples with a depth of 2–20 um exhibited nearly 20% improvement in spectral transmission relative to the planar baseline in the range of wavelength of light 300–650 nm. The percentage of spectral transmission at 650 nm for all samples in Figures 3 and 4 displayed almost the same value of about 95% to 99%. However, differences in the spectral transmission percentage were observed when the wavelength of light increased from 650 nm to the infrared range. The percentage of spectral transmission for Samples E (base angle of 26.57º), M (base angle of 26.57º) and N (base angle of 21.80º) declined relative to the planar baseline.

In addition, Samples M and N that had a base angle below 30° showed almost the same pattern as the planar baseline, and they had a low percentage of spectral transmission compared with Sample J (period of 20 μm with depth of 20 μm), K (period of 40 μm with depth of 20 μm) and L (period of 60 μm with depth of 20 μm). This result is obtained because the structure of texturization for Sample N had a wide base height and low pyramidal depth, which contributed to numerous losses in incident light on the

planar surface compared with Sample K. These samples require an encapsulant with increasingly high refractive index to navigate the internal reflection between the air–glass interface of light initially reflected from the cell surface when the base angle is reduced from an optimised angle to a small one. Therefore, the base angle of the pyramidal texture should be considered when analysing light-trapping, photo-generation and surface recombination properties.

Figure 6(a) and 6(b) present the spectral transmission of reflected and collected incident light (photon) on the front surface of the solar cell shown in Figure 2 respectively. These data were selected from the results in Figure 3 because they showed good performance in spectral transmission. The spectral reflectance in Figure 6(a) shows the reflection losses in Samples A, F, G, H, J, K, L and the planar baseline. The planar baseline showed huge differences in reflectance of around 25% relative to the other pyramidal textures in the range of wavelength of light 300–600 nm. The other pyramidal textured surfaces exhibited almost the same reflectance on the front surface. Sample F manifested slightly more reflectance than the other pyramidal textured samples in the range of wavelength of light of 380–560 nm with variance of 6%. The impact of the pyramidal textured structure showed a significant potential to limit the direct reflection of light from the textured surface [20]. Moreover, the reflectance of light for the planar and pyramidal textured surfaces in the range of wavelength of light of 600–680 nm was the same, which reached nearly zero reflectance. However, differences in reflectance were observed between the planar and pyramidal textured surfaces when the wavelength of light reached the infrared range. The reduction in front surface reflectance is important to improve the photo-generation current of c-Si solar cells. Thus, the improvement in reflectance in Samples A, F, G, H, J, K and L was the result of the pyramidal texture serving its purpose in light trapping and increasing the front surface area so that more incident light can be extracted. In addition, reducing the reflectance on the Si surface can enhance the light absorbance and rate generation (spectral collection probability) of electron-hole pairs [21–22].

Figure 6(b) presents the percentage of incident light collected by the solar cell devices with respect to the wavelength of light. All pyramidal textured samples, except for A, exhibited higher spectral collection probability than the planar surface in the visible and infrared ranges. The spectral collection by Sample A (period of 4 μm with depth of 4 μm) was slightly higher than that for the planar surface in the range of wavelength of light of 400–700 nm with 2% improvement. It also showed less spectral collection in the infrared range. The higher surface recombination on the planar surface than in Sample A (period of 4 μm with depth of 4 μm) caused the collection probability on the surface to be low due to more reflectance. Meanwhile, Samples F (period of 8 μm with depth of 4 μm), G (period of 8 μm with depth of 8 μm), H (period of 8 μm with depth of 8 μm), J (period of 20 μm with depth of 20 μm), K (period of 40 μm with depth of 20 μm) and L (period of 60 μm with depth of 20 μm) had high collection probability on the front surface, which reduced surface recombination. These samples had more carriers generated by light absorption on the front surface that were collected by the p-n junction. These carriers contributed to the light-generated current. The properties of the front surface exerted a huge impact on the collection probability of the device because when the carriers were generated in the region with higher recombination than the junction, the probability of carrier recombination was high. Afterwards, the front surface was passivated with thin interfacial oxide and positive-charge silicon nitride for anti-reflection

coating, which prevented the electrons and holes from recombining prematurely on the front surface. The passivation of the SiO_2/SiN_x stack is known as effective surface passivation [23]. One of the properties of SiO_2 is to improve the passivation quality of textured front surfaces with emitters for n- and p-type silicon surfaces as well as the rear surface [24–28].

Figures 7 and 8 show the graphical output for mobility and carriers inside the silicon wafer together with the collection probability respectively, all of which affect the output of the silicon solar cell. Both samples had different structures on the front surface of the silicon wafer. The intensity of the mobility and carriers inside a silicon cell is determined by the thickness of the concentration from the top to the bottom of the silicon wafer. The higher the concentration intensity of the mobility and carriers is in the silicon wafer, the more minority carriers are created, absorbed and collected and the fewer the reflection losses that occur on the front surface. The planar surface had smaller mobility and carrier thickness than Sample J (period of 20 μm with depth of 20 μm), which appeared to have larger mobility and carrier thickness around the front surface of the pyramidal texture that exhibited many photons of a given incident energy in the solar cell devices. Consequently, many minority carriers were generated and collected by the silicon wafer due to the enhancement of pyramidal textured and passivated front surface. The passivated and pyramidal textured front surface showed that photons were not reflected nor transmitted out of the cell, which created collectable carriers.

Figure 9(a) and 9(b) presents the electric field and velocity from the top to the bottom of the pyramidal texture in Samples F and J respectively. In the presence of the electric field, drift velocity occurred during the mobility of the charge carrier. The impact of mobility with respect to drift velocity and the electric field was significant in absorbing the sunlight at maximum capacity and avoiding surface recombination. Figure 9(a) shows the occurrence of the electric field in the planar baseline, Sample F (period of 8 μm with depth of 4 μm) and Sample J (period of 20 μm with depth of 20 μm) with depth in the wafer from top to bottom. The electric field in Samples F and J was higher than that in the planar sample due to the strong presence of opposite-charge ions that prevented electrons in the n-type layer from filling the holes in the p-type layer. In addition, the electric field transported the electrons from the n-type layer and holes to the p-type layer as the electrons in the silicon were ejected from their original places when the energy of sunlight was equal to or more than the energy bandgap of silicon strikes on the front surface of the solar cell. Regardless of the presence of an electric field, the different conductivity of the electrons and holes in two regions had a significant impact on charge carrier separation in the solar cell [29]. The electric field had a significant effect on enhancing short-circuit current density when bias-dependent carrier multiplicity was considered [30].

Figure 9(b) shows the velocity inside the planar and pyramidal textures with depth in the wafer from top to bottom. Carrier mobility occurred when the electric field was applied on the silicon, making the electrons move in the direction opposite of the electric field whilst the holes moved around in the net direction of the electric field. The velocity in Sample J (period of 20 μm with depth of 20 μm) was much higher than that in Sample F (period of 8 μm with depth of 4 μm) and the planar sample because of the correlation with the electric field produced in each sample. This result is due to the electric field present

inside the silicon wafer. Carriers move in the net direction because of the presence of an electric field and thermal velocity. Balancing of carrier velocity by enhancing the driving field improves the conversion efficiency of solar cells because the driving field is required for migrating the optically generated holes [31].

Figure 10(a) and 10(b) present the current and surface recombination from top to bottom of the pyramidal texture in the planar sample and Samples F and J respectively. As indicated in Figure 10(a), the current produced by Sample J was 2.30E-04 A/cm^2, which is much higher than that of Sample F (8.27E-05 A/cm^2) and the planar sample (3.77E-05 A/cm^2). This result is correlated to the electric field and velocity of the mobility of the charge carrier in Figure 6. The photons absorbed by the silicon wafer that generated electron-hole pairs in the minority charge carriers made the transition to the depletion region by the diffusion caused by drift with the presence of the internal electric field. Thus, when no recombination of the charge carriers with the majority carriers occurred in the quasi-neutral regions, the electric field of the depletion region moved the minority carriers to the other side of the junction. Consequently, electrical current was generated by the minority carriers inside the silicon wafers.

Figure 10(b) shows the surface recombination in the planar, F and J samples with respect to depth in the wafer from top to bottom. The planar sample exhibited more surface recombination than Samples F and J (i.e., 1.79E13 cm^{-2}/s). The surface recombination between Samples F and J was small with a value of 1.04E13 and 1.09E13 cm^{-2}/s, respectively. The large differences in surface recombination between the planar and pyramidal textures were caused by the lack of light trapping and abundant reflectance on the front surface of the planar surface. Notably, a planar surface without any additional rough surface acts as a mirror that reflects incident light, whereas a pyramidal textured surface traps the incident light inside and reflects it to the neighbouring pyramidal texture before being reflected back to air. In addition, surface recombination is proportionally dependent on surface roughness, contamination, amount of surface area between the absorbing Si and the extracting contact and ambient gases used during oxidation and annealing [32-33].

Pyramidal texturization's size and shape exert a huge influence on controlling the effectiveness of the anti-reflection effect. Thus, for low reflectance over a large range of wavelength, the size and shape of pyramidal texturization are crucial. The main function of pyramidal texturization is to increase the transmission of incoming photons into silicon. When incident light strikes on a pyramidal textured surface, some of it is reflected and some is transmitted, thus achieving this function. Reflected light hits the neighbouring pyramidal texture and is partly reflected back and coupled into silicon. This reflected light shows an improvement in the pyramidal texture over the planar surface.

Pyramidal texturization alone or with anti-reflection coating reduces reflection losses on the front surface of silicon cells. Texturization decreases the reflection of incident photons by enhancing the reflected light bouncing back on the textured surface, thus minimising the reflection on the planar surface. Figure 11 shows how incident light strikes on the planar and pyramidal textured surfaces. The movement of incident light on the planar surface showed that when incoming light struck the surface and

was reflected back to the surrounding air, R varied from 0 to 1. By contrast, rather than being lost as that on the planar surface, the incoming light reflected by the pyramidal textured surface hit the neighbouring pyramid texture, resulting in a reduction of reflection losses to R2I.

Conclusion

Spectral transmission on planar and pyramidal textured silicon wafers was studied using a new simulation software known as PC3S. This is the first time the PC3S software package has been utilised for research. All parameters were fixed, and the size of pyramidal texturization varied. The introduction of this software to the modelling of the performance of surface silicon cells is crucial in the photovoltaic field because it aids in the basic understanding of the influence of surface texturization.

Declarations

We confirm that the manuscript has been read and approved by all named authors and that there are no other persons who satisfied the criteria for authorship but are not listed. We further confirm that the order of authors listed in the manuscript has been approved by all of us. This research paper has not been previously published and is not currently under consideration by another journal. All authors have played their roles to produce this research paper. Thus, all authors have approved and agreed to submit this paper to this journal.

Author's contribution

All the authors have made substantial contribution regarding all the simulation modelling and data analysis also drafting and revising the manuscript. We confirm that the manuscript has been read and approved by all named authors and that there are no other persons who satisfied the criteria for authorship but are not listed. We further confirm that the order of authors listed in the manuscript has been approved by all of us. This research paper has not been previously published and is not currently under consideration by another journal. All authors have played their roles to produce this research paper. Thus, all authors have approved and agreed to submit this final paper to this journal.

Competing interest

Other than the grants listed in the acknowledgement section, the authors declare that they have no other competing interests.

Availability of data

Data can be shared upon request.

Funding

Publication of this article was funded by Laboratory Research Grant Scheme (LRGS/1/2019/UKM-UKM/6/1).

Acknowledgement

This work has been carried out with the support of the Laboratory Research Grant Scheme (LRGS/1/2019/UKM-UKM/6/1). Thanks for Ministry of Education, Malaysia, and University Sains Malaysia to give sponsorship for my PhD studies at Solar Energy Research Institute (SERI), UKM.

Compliance with Ethical Standards Affiliations

Disclosure of potential conflicts of interest

The simulation used in this paper is free simulation and creator of this simulation is well cited.

Research involving Human Participants and/or Animals

Not applicable.

Informed consent

Not applicable.

Consent to participate and Consent for publication

Not applicable.

References

[1] T. M. Razykov, C. S. Ferekides, D. Morel, E. Stefanakos, H. S. Ullal, and H. M. Upadhyaya, “Solar photovoltaic electricity: Current status and future prospects,” *Sol. Energy*, vol. 85, no. 8, pp. 1580–1608, 2011, doi: 10.1016/j.solener.2010.12.002.

[2] M. Berginski *et al.*, “Experimental studies and limitations of the light trapping and optical losses in microcrystalline silicon solar cells,” *Sol. Energy Mater. Sol. Cells*, vol. 92, no. 9, pp. 1037–1042, 2008, doi: 10.1016/j.solmat.2008.03.005.

[3] L. L. Ma *et al.*, “Wide-band ‘black silicon’ based on porous silicon,” *Appl. Phys. Lett.*, vol. 88, no. 17, 2006, doi: 10.1063/1.2199593.

[4] S. H. Zaidi, J. M. Gee, and D. S. Ruby, “Diffraction grating structures in solar cells,” *Conf. Rec. IEEE Photovolt. Spec. Conf.*, vol. 2000-Janua, pp. 395–398, 2000, doi: 10.1109/PVSC.2000.915850.

[5] M. K. Basher, M. K. Hossain, and M. A. R. Akand, “Effect of surface texturization on minority carrier lifetime and photovoltaic performance of monocrystalline silicon solar cell,” *Optik (Stuttg).*, vol. 176, no. July 2018, pp. 93–101, 2019, doi: 10.1016/j.ijleo.2018.09.042.

[6] J. Cichoszewski, M. Reuter, and J. H. Werner, “+0.4% Efficiency gain by novel texture for String Ribbon solar cells,” *Sol. Energy Mater. Sol. Cells*, vol. 101, pp. 1–4, 2012, doi: 10.1016/j.solmat.2012.01.031.

[7] M. Moreno *et al.*, “A comparative study of wet and dry texturing processes of c-Si wafers for the fabrication of solar cells,” *Sol. Energy*, vol. 101, pp. 182–191, 2014, doi: 10.1016/j.solener.2014.01.004.

[8] A. Bougoffa, A. Trabelsi, A. Zouari, and E. Dhahri, “Analytical model of front texturization effect on silicon solar cell with porous silicon at the backside,” *Opt. Quantum Electron.*, vol. 49, no. 1, pp. 1–13, 2017, doi: 10.1007/s11082-016-0864-8.

[9] M. K. Basher, M. K. Hossain, M. J. Uddin, M. A. R. Akand, and K. M. Shorowordi, “Effect of pyramidal texturization on the optical surface reflectance of monocrystalline photovoltaic silicon wafers,” *Optik (Stuttg).*, vol. 172, pp. 801–811, 2018, doi: 10.1016/j.ijleo.2018.07.116.

[10] E. Y. Plotnikova, A. V Arsentiev, and M. E. Harchenko, “Textured solar cell modeling in TCAD,” *IOP Conf. Ser. Mater. Sci. Eng.*, vol. 1035, no. 1, p. 012002, 2021, doi: 10.1088/1757-899x/1035/1/012002.

[11] C. Jin, I. Martín, P. R. Ortega, E. Calle, and R. Alcubilla, “3D simulations of interdigitated back-contacted crystalline silicon solar cells on thin substrates,” *Sol. Energy*, vol. 167, no. January, pp. 242–250, 2018, doi: 10.1016/j.solener.2018.04.022.

[12] S. Ma *et al.*, “A theoretical study on the optical properties of black silicon,” *AIP Adv.*, vol. 8, no. 3, 2018, doi: 10.1063/1.5018642.

[13] D. Pera, G. Gaspar, K. Lobato, and I. Costa, “COMPUTATIONAL OPTICAL ANALYSIS OF 3D MODELED CRYSTALLINE,” no. November, pp. 2–5, 2020, doi: 10.4229/EUPVSEC20202020-2CV.1.16.

[14] D. K. Shah, J. Choi, D. Kc, M. S. Akhtar, C. Y. Kim, and O. B. Yang, “Refined optoelectronic properties of silicon nanowires for improving photovoltaic properties of crystalline solar cells: a simulation study,” *J. Mater. Sci. Mater. Electron.*, no. February, 2021, doi: 10.1007/s10854-020-05031-w.

[15] H. D. Omar, M. R. Hashim, and M. Z. Pakhuruddin, “Ray tracing of inverted pyramids for light-trapping in thin crystalline silicon for solar cells,” *Optik (Stuttg).*, vol. 219, no. July, p. 165279, 2020, doi: 10.1016/j.ijleo.2020.165279.

[16] P. A. Basore, “PC3S.” 2020.

[17] Z. Mrazkova, I. P. Sobkowicz, and M. Foldyna, “Optical properties and performance of pyramidal texture silicon heterojunction solar cells : Key role of vertex angles,” no. January, pp. 1–8, 2018, doi: 10.1002/pip.2994.

[18] K. R. M. Simeon C. Baker-Finch, “Reflection distributions of textured monocrystalline silicon-Implications for silicon solar cells,” *Prog. PHOTOVOLTAICS Res. Appl.*, vol. 20, no. 6, pp. 1114–1129, 2012, doi: 10.1002/pip.

[19] G. Hashmi, A. R. Akand, M. Hoq, and H. Rahman, “Study of the Enhancement of the Efficiency of the Monocrystalline Silicon Solar Cell by Optimizing Effective Parameters Using PC1D Simulation,” *Silicon*, vol. 10, no. 4, pp. 1653–1660, 2018, doi: 10.1007/s12633-017-9649-3.

[20] M. Ju *et al.*, “Influence of small size pyramid texturing on contact shading loss and performance analysis of Ag-screen printed mono crystalline silicon solar cells,” *Mater. Sci. Semicond. Process.*, vol. 85, no. April, pp. 68–75, 2018, doi: 10.1016/j.mssp.2018.05.039.

[21] J. Zhao, A. Wang, P. P. Altermatt, S. R. Wenham, and M. A. Green, “24% Efficient perl silicon solar cell: Recent improvements in high efficiency silicon cell research,” *Sol. Energy Mater. Sol. Cells*, vol. 41–42, pp. 87–99, 1996, doi: 10.1016/0927-0248(95)00117-4.

[22] K. Forberich, G. Dennler, M. C. Scharber, K. Hingerl, T. Fromherz, and C. J. Brabec, “Performance improvement of organic solar cells with moth eye anti-reflection coating,” *Thin Solid Films*, vol. 516, no. 20, pp. 7167–7170, 2008, doi: 10.1016/j.tsf.2007.12.088.

[23] J. Schmidt, R. Peibst, and R. Brendel, “Surface passivation of crystalline silicon solar cells: Present and future,” *Sol. Energy Mater. Sol. Cells*, vol. 187, pp. 39–54, 2018, doi: 10.1016/j.solmat.2018.06.047.

[24] Y. L. Chen, G. L. Lu, S. H. Zhong, and W. Z. Shen, “SiO2 Passivation Layer Grown by Liquid Phase Deposition for N-type Bifacial Silicon Solar Cells,” *MATEC Web Conf.*, vol. 67, 2016, doi: 10.1051/matecconf/20166704008.

[25] T. Jana, S. Mukhopadhyay, and S. Ray, “Low temperature silicon oxide and nitride for surface passivation of silicon solar cells,” *Sol. Energy Mater. Sol. Cells*, vol. 71, no. 2, pp. 197–211, 2002, doi: 10.1016/S0927-0248(01)00058-7.

[26] S. MacK *et al.*, “Properties of purified direct steam grown silicon thermal oxides,” *Sol. Energy Mater. Sol. Cells*, vol. 95, no. 9, pp. 2570–2575, 2011, doi: 10.1016/j.solmat.2011.03.002.

[27] S. MacK *et al.*, “Silicon surface passivation by thin thermal oxide/PECVD layer stack systems,” *IEEE J. Photovoltaics*, vol. 1, no. 2, pp. 135–145, 2011, doi: 10.1109/JPHOTOV.2011.2173299.

[28] N. M. Terlinden, G. Dingemans, V. Vandalon, R. H. E. C. Bosch, and W. M. M. Kessels, “Influence of the SiO2 interlayer thickness on the density and polarity of charges in Si/SiO2/Al2O3 stacks as studied by optical second-harmonic generation,” *J. Appl. Phys.*, vol. 115, no. 3, 2014, doi: 10.1063/1.4857075.

[29] U. Wurfel, A. Cuevas, and P. Wurfel, “Charge carrier separation in solar cells,” *IEEE J. Photovoltaics*, vol. 5, no. 1, pp. 461–469, 2015, doi: 10.1109/JPHOTOV.2014.2363550.

[30] M. Faye, C. Mbow, and B. Ba, “Internal Electric Field In The Space Charge Layer Of A Solar Cell Based On Silicon In The Presence Of Excitons,” *Int. J. Sci. Technol. Res.*, vol. 4, no. 10, pp. 66–69, 2015.

[31] C. T. Lee, K. F. Lu, and C. Y. Tseng, “Carrier drift velocity balance mechanism in Si-based thin film solar cells using graded microcrystalline SiGe absorption layer,” *Sol. Energy*, vol. 114, pp. 1–7, 2015, doi: 10.1016/j.solener.2015.01.023.

[32] A. Belghachi, “Detailed analysis of surface recombination in crystalline silicon solar cells,” *Proc. 2013 Int. Renew. Sustain. Energy Conf. IRSEC 2013*, pp. 161–166, 2013, doi: 10.1109/IRSEC.2013.6529729.

[33] J. Wang, W. Fu, S. Jariwala, I. Sinha, A. K. Y. Jen, and D. S. Ginger, “Reducing Surface Recombination Velocities at the Electrical Contacts Will Improve Perovskite Photovoltaics,” *ACS Energy Lett.*, vol. 4, no. 1, pp. 222–227, 2019, doi: 10.1021/acsenergylett.8b02058.

Tables

Table 1. Silicon parameter

Silicon surface morphology parameters	Values
Wafer type	Silicon *P*-type
Contact mode	Bipolar
Illumination	Dark
Base doping	1.0×10^{16} cm^{-3}
Diffusion peak	2.0×10^{19} cm^{-3}
Diffusion type	n
Diffusion shape	Gaussian
Charge shape	Uniform
Permittivity	11.9
Peak SRV	1000 cm/s
Valley SRV	1000 cm/s
SRVshape	Uniform
Temperature	25°C

Table 2. Textured surface morphology of silicon parameter

Sample	Base length (half period) pyramidal, μm	Period, μm	Depth, μm	Base angle, θ
A	2	4	4	63.44
B	2	4	6	71.57
C	2	4	8	75.96
D	2	4	10	78.69
E	4	8	2	26.57
F	4	8	4	45.00
G	4	8	6	56.31
H	4	8	8	63.44
I	4	8	10	68.20
J	10	20	20	63.44
K	20	40	20	45.00
L	30	60	20	33.69
M	40	80	20	26.57
N	50	100	20	21.80

Figures

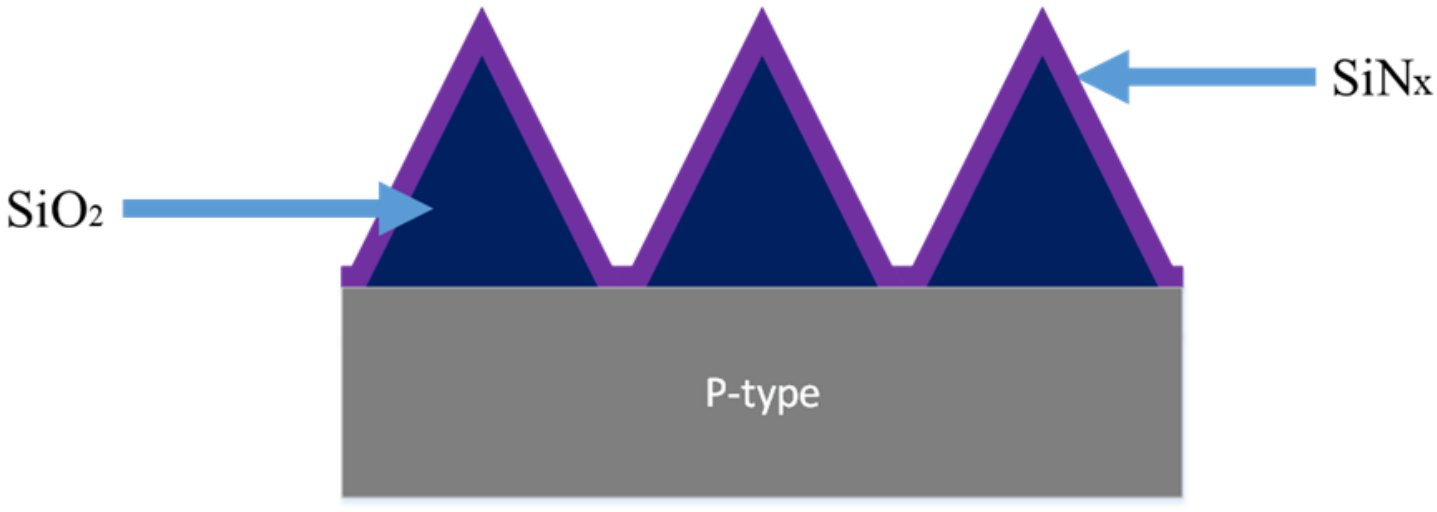

Figure 1

Configuration of the period and depth of pyramidal textured

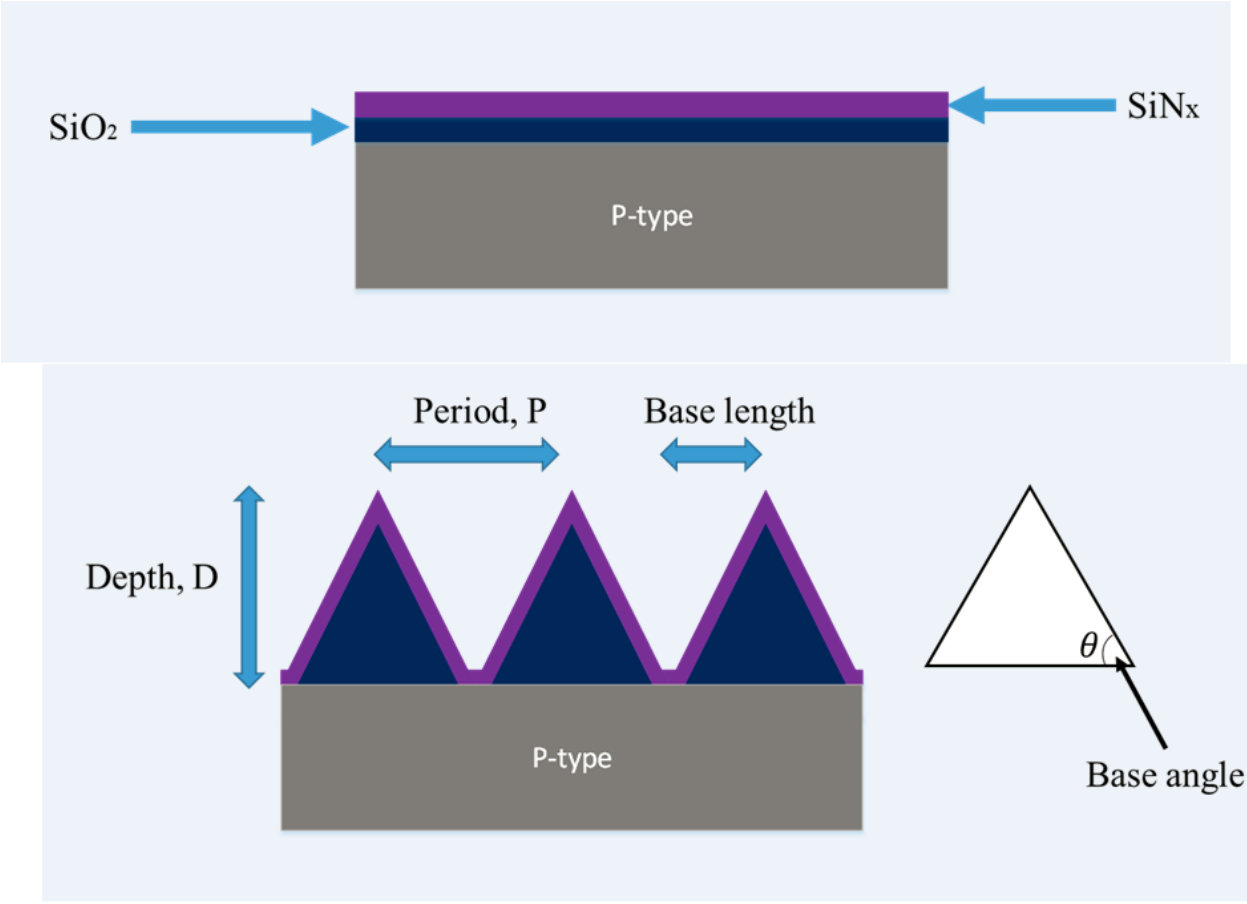

Figure 2

Schematic surface morphology of silicon wafer used in the simulation (a) planar and (b) textured

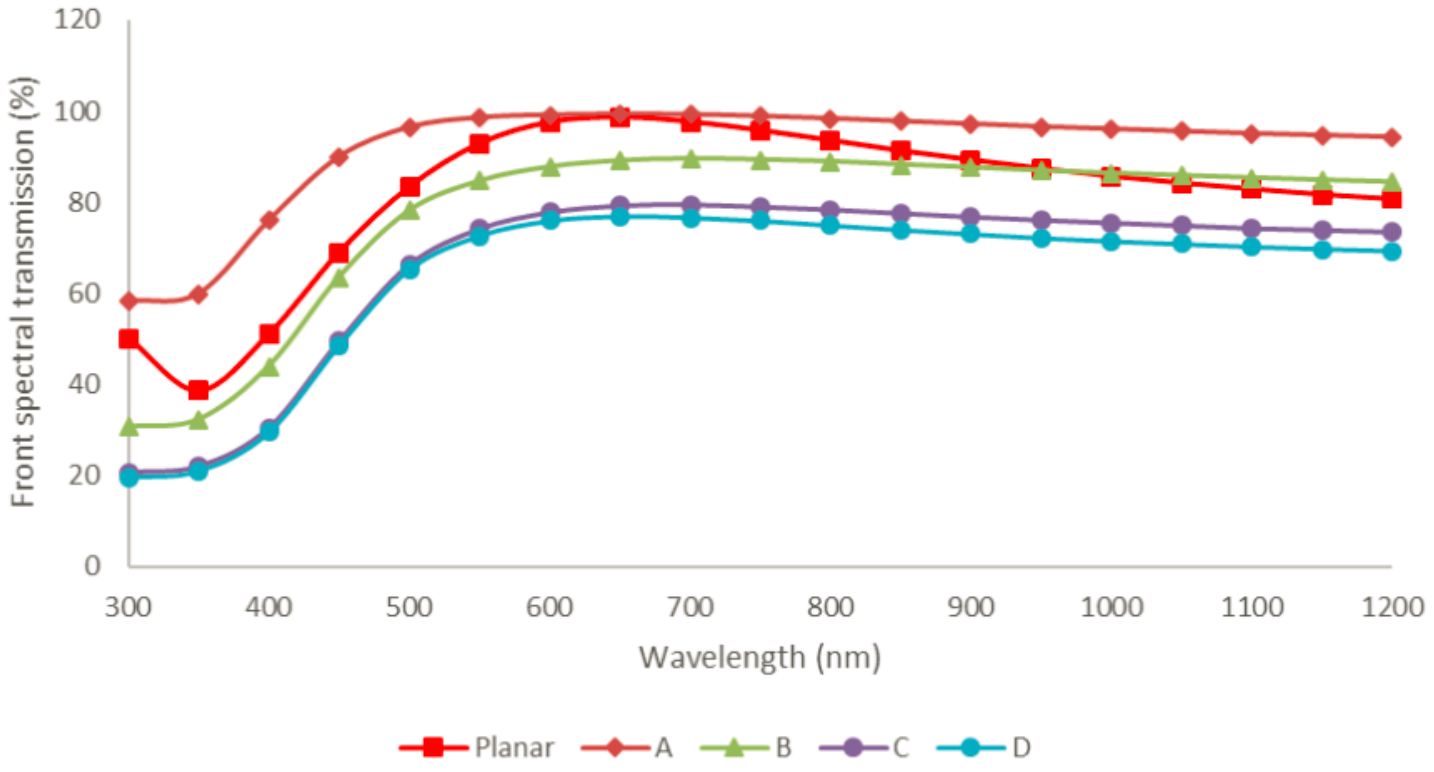

Figure 3

Percentage of front surface spectral transmission on textured surface with period of 4um

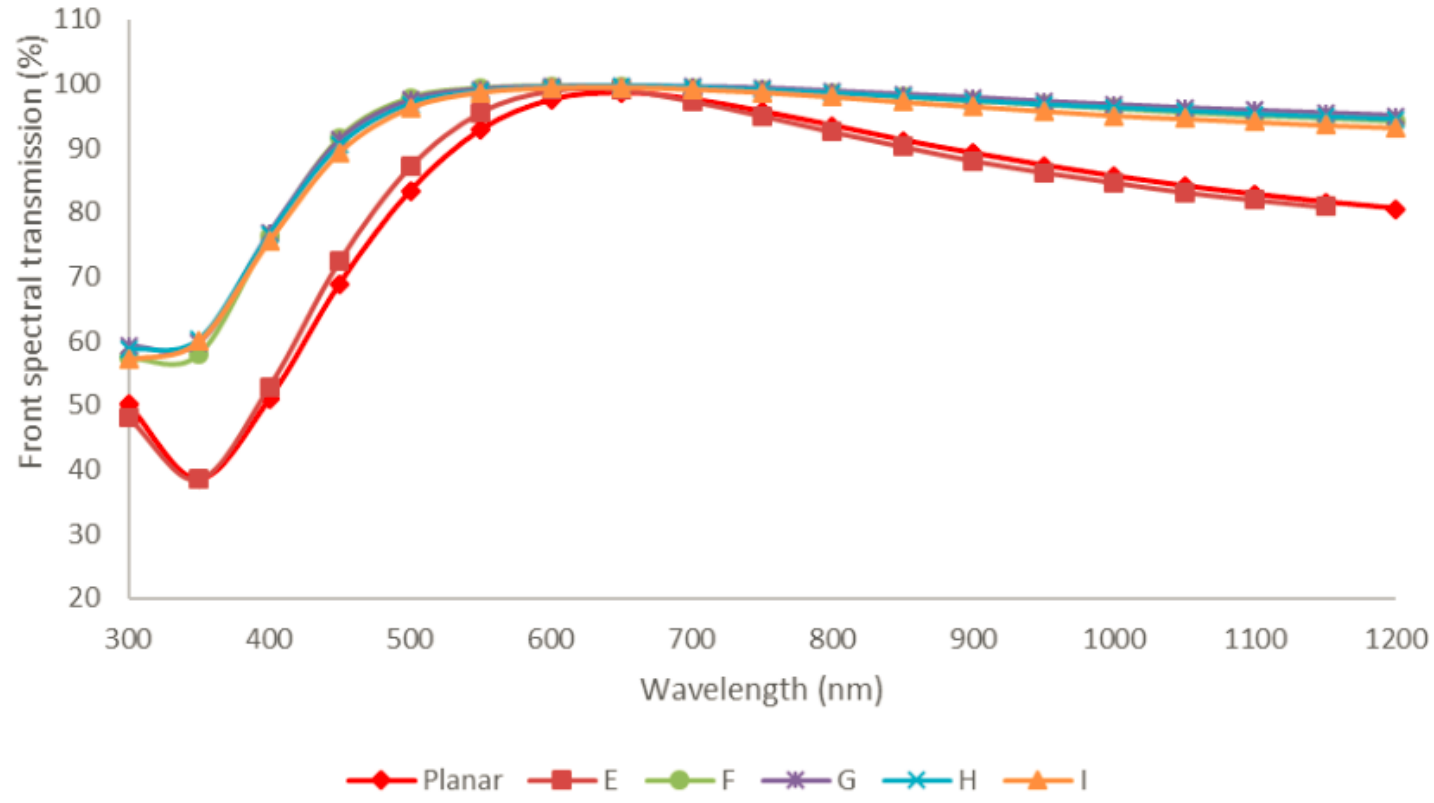

Figure 4

Percentage of front surface spectral transmission on textured surface with period of 8um

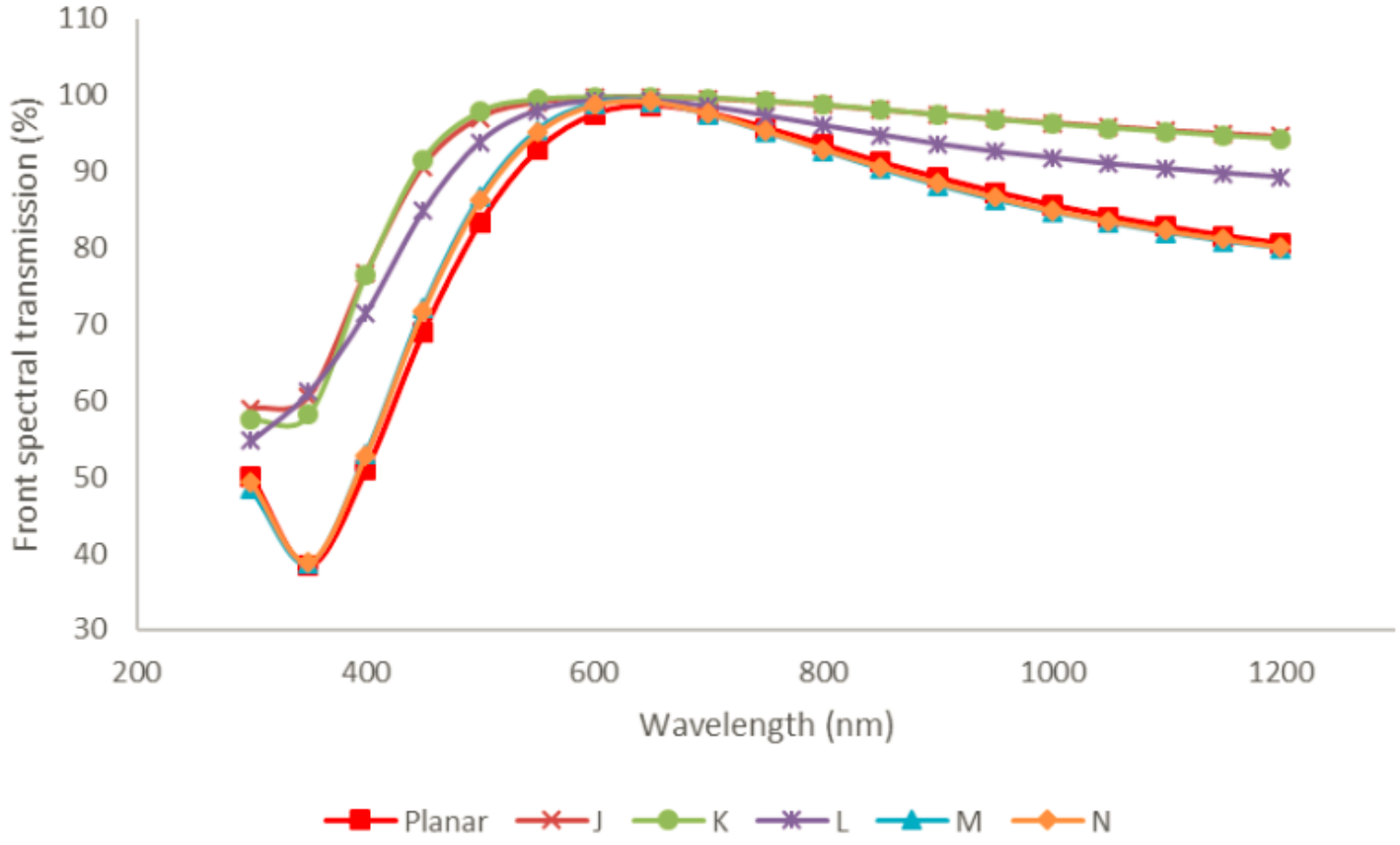

Figure 5

Percentage of front surface spectral transmission on textured surface with period of 20um

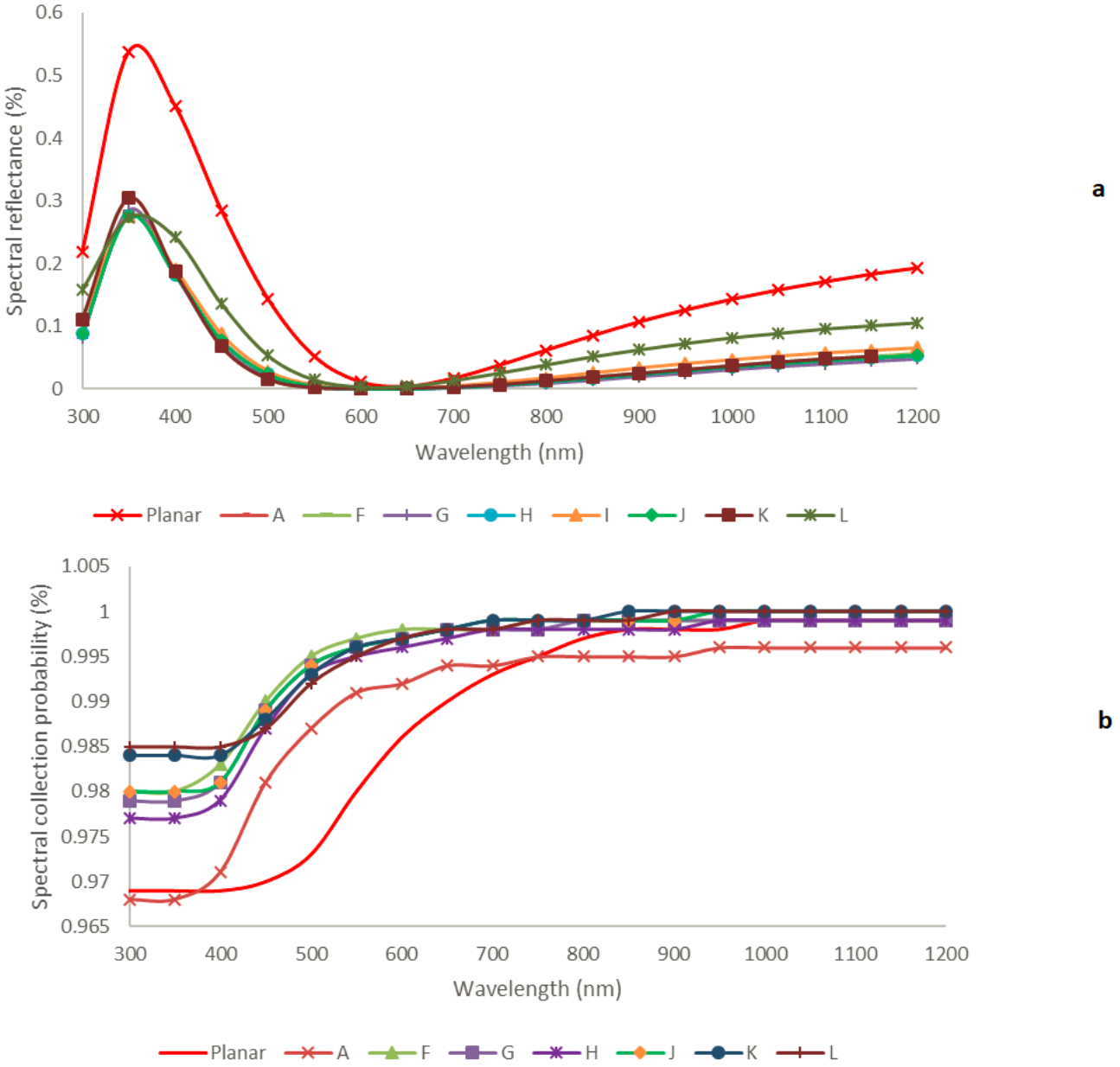

Figure 6

Spectral (a) reflected and (b) collected on the pyramidal textured solar cell device by PC3S simulation

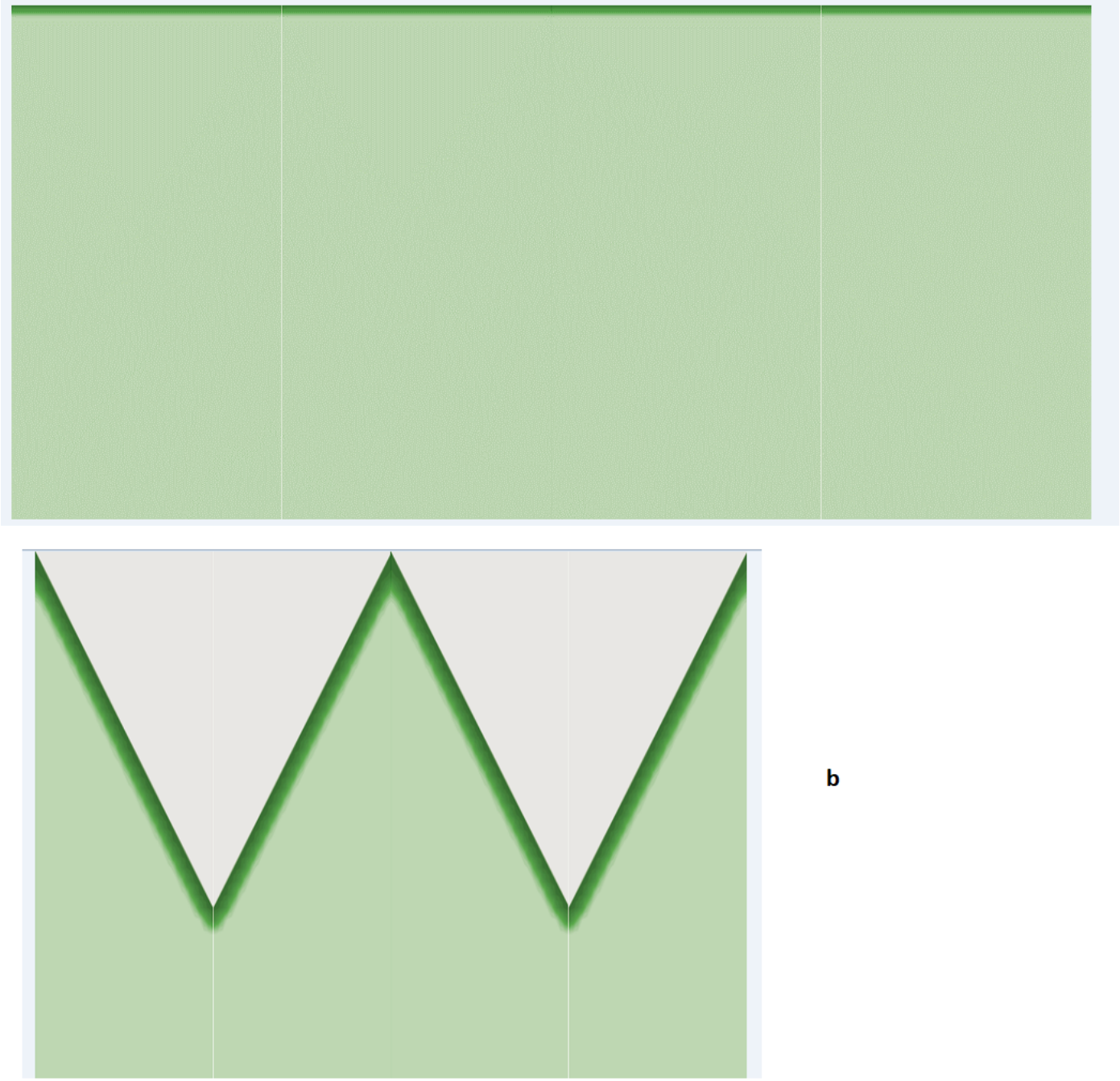

Figure 7

Mobility on silicon cell for sample (a) planar and (b) J (P20D20)

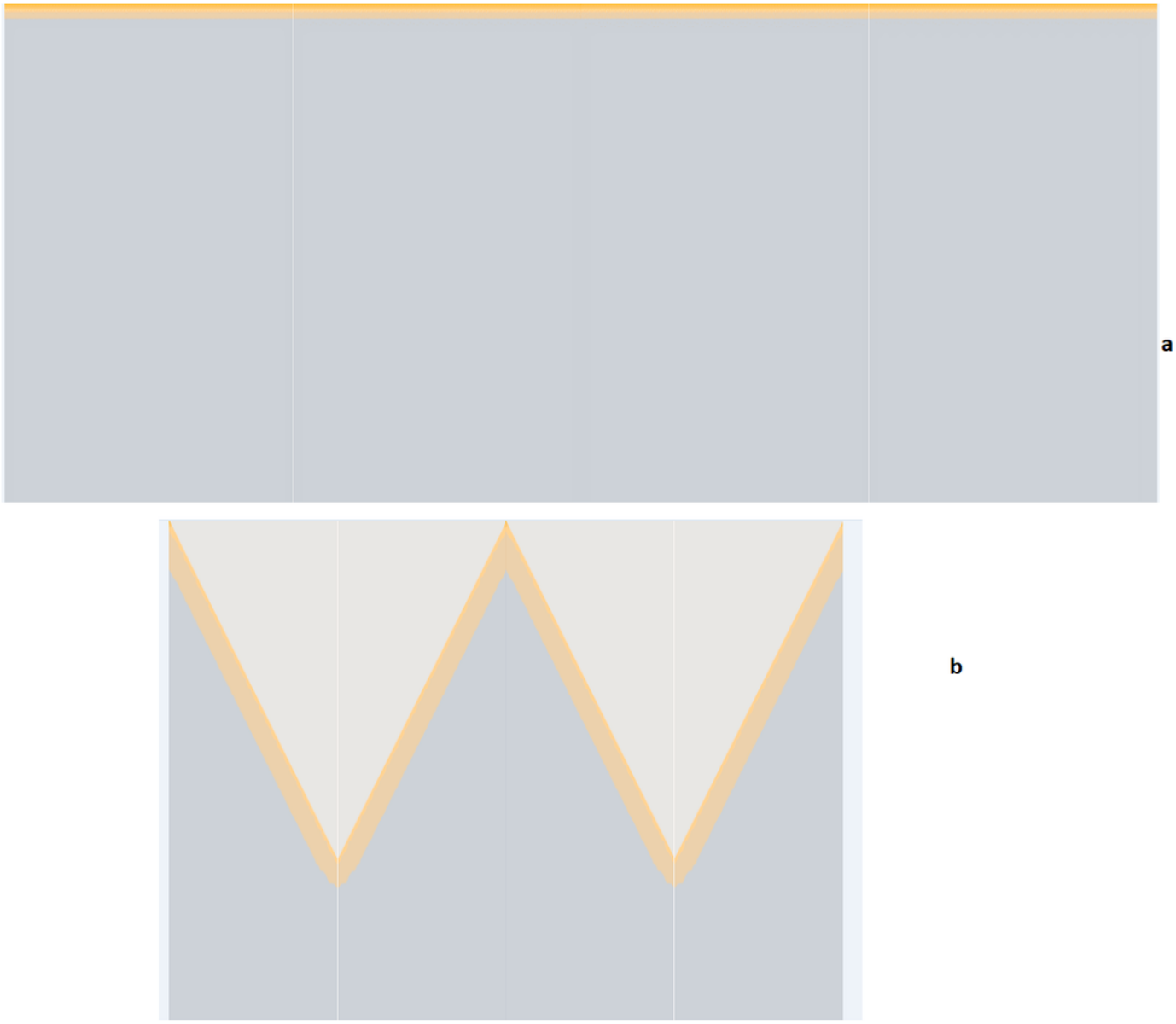

Figure 8

Carriers on silicon cell for sample (a) planar and (b) J (P20D20)

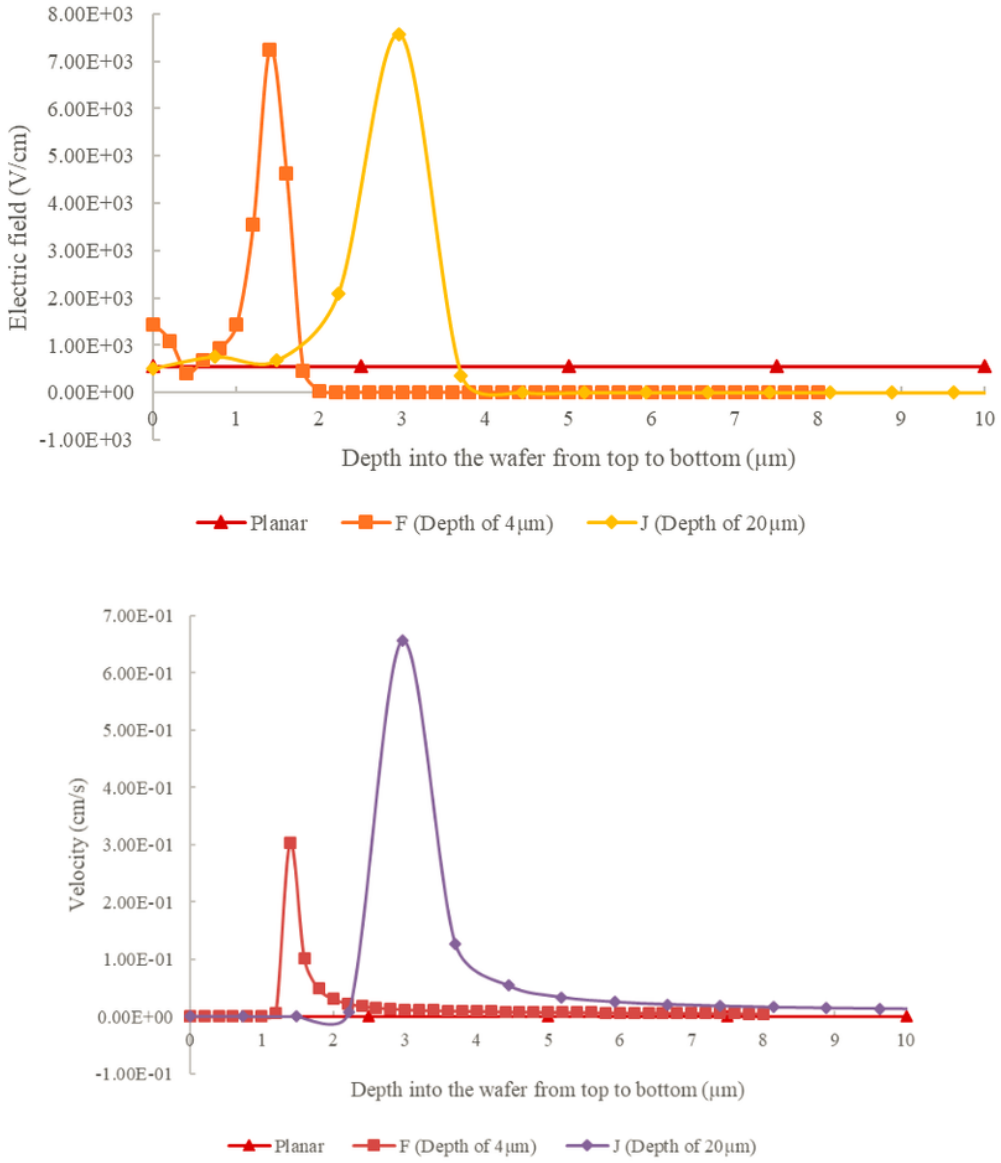

Figure 9

Graph of (a) electric field and (b) velocity for planar, F, and J samples

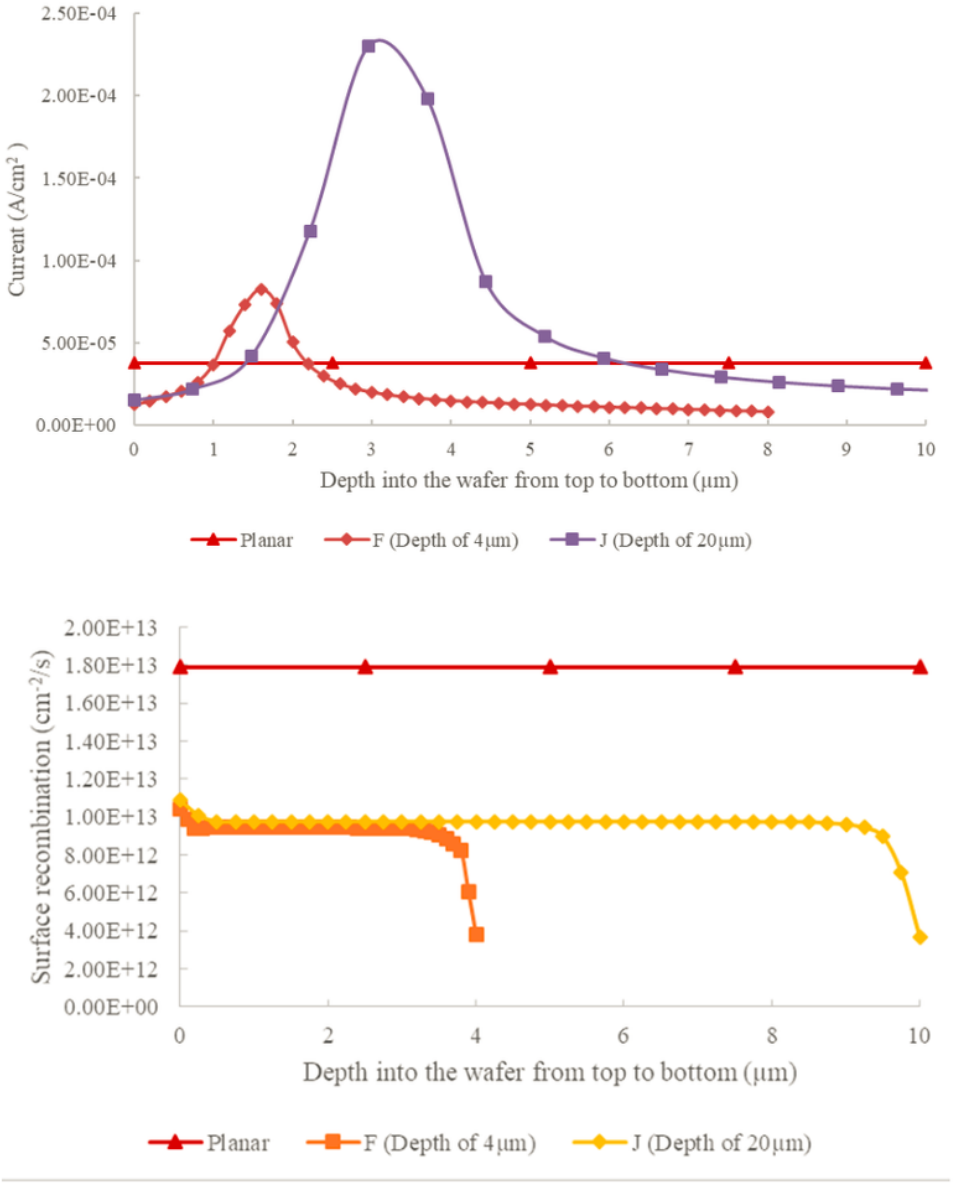

Figure 10

Graph of (a) current, and (b) surface recombination for planar, F, and J samples

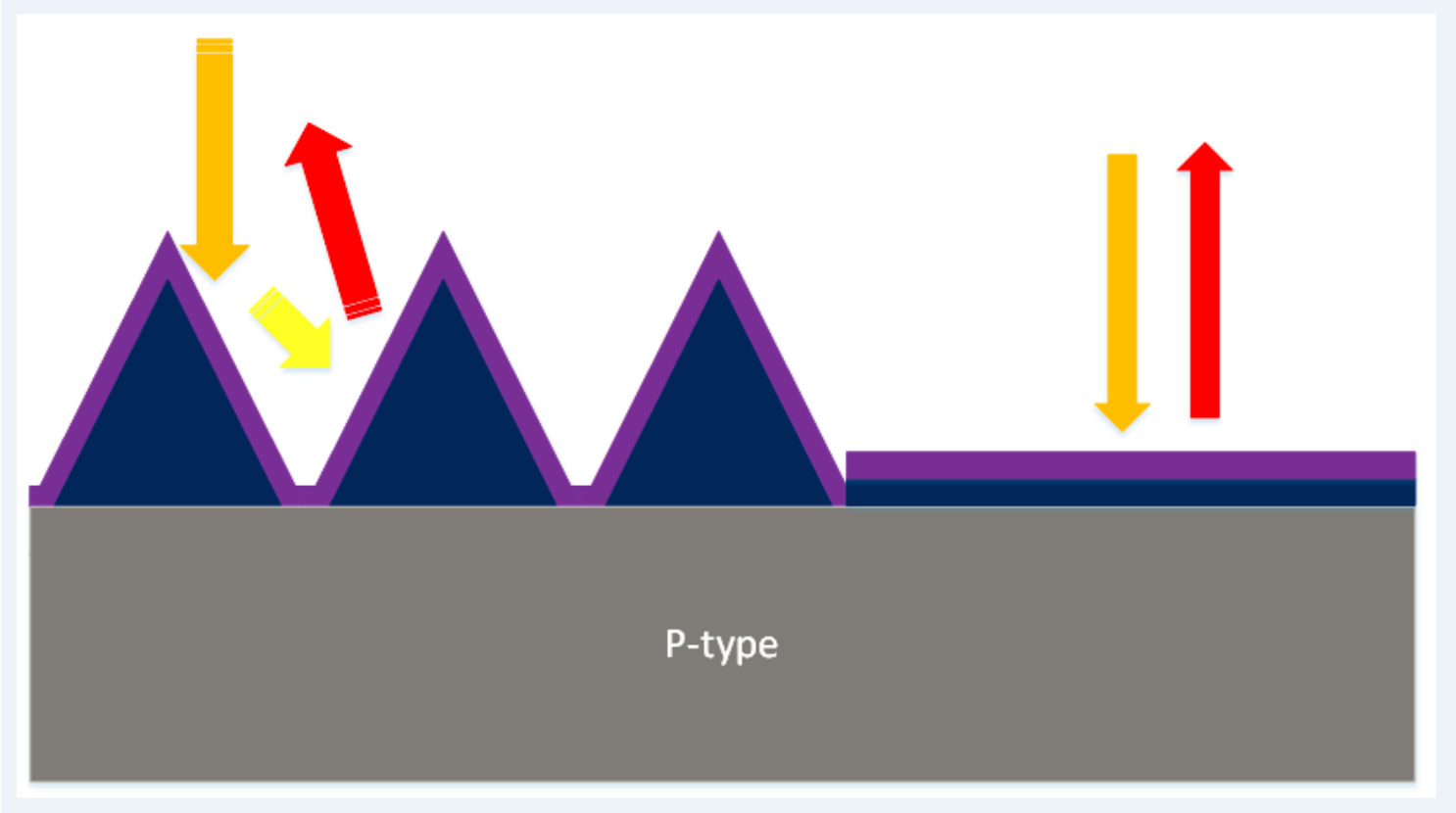

Figure 11

Movement of incident light strikes on the planar and pyramidal textured surface